



A record of plume-induced plate rotation triggering subduction initiation

Douwe J. J. van Hinsbergen¹✉, Bernhard Steinberger^{2,3}, Carl Guilmette⁴, Marco Maffione^{1,5}, Derya Gürer^{1,6}, Kalijn Peters¹, Alexis Plunder^{1,7}, Peter J. McPhee¹, Carmen Gaina^{3,8}, Eldert L. Advokaat^{1,5}, Reinoud L. M. Vissers¹ and Wim Spakman¹

The formation of a global network of plate boundaries surrounding a mosaic of lithospheric fragments was a key step in the emergence of Earth's plate tectonics. So far, propositions for plate boundary formation are regional in nature; how plate boundaries are created over thousands of kilometres in geologically short periods remains elusive. Here we show from geological observations that a >12,000-km-long plate boundary formed between the Indian and African plates around 105 Myr ago. This boundary comprised subduction segments from the eastern Mediterranean region to a newly established India–Africa rotation pole in the west Indian Ocean, where it transitioned into a ridge between India and Madagascar. We identify coeval mantle plume rise below Madagascar–India as the only viable trigger of this plate rotation. For this, we provide a proof of concept by torque balance modelling, which reveals that the Indian and African cratonic keels were important in determining plate rotation and subduction initiation in response to the spreading plume head. Our results show that plumes may provide a non-plate-tectonic mechanism for large-plate rotation, initiating divergent and convergent plate boundaries far away from the plume head. We suggest that this mechanism may be an underlying cause of the emergence of modern plate tectonics.

The early establishment of plate tectonics on Earth was likely a gradual process that evolved as the cooling planet's lithosphere broke into a mosaic of major fragments, separated by a network of plate boundaries: spreading ridges, transform faults and subduction zones¹. The formation of spreading ridges and connecting transform faults is regarded as a passive process, occasionally associated with rising mantle plumes². The formation of subduction zones is less well understood. Explanations for subduction initiation often invoke spontaneous gravitational collapse of ageing oceanic lithosphere² or relocations of subduction zones due to intraplate stress changes in response to arrival of continents, oceanic plateaus or volcanic arcs in trenches³. Mantle plumes have also been suggested as drivers for regional subduction initiation, primarily based on numerical modelling^{4–6}. But while such processes may explain how plate tectonics evolves on a regional scale, they do not provide insight into the geodynamic cause(s) for the geologically sudden (<10 Myr) creation of often long (>1,000 km) plate boundaries including new subduction zones⁷. Demonstrating the causes of plate boundary formation involving subduction initiation using the geological record is challenging and requires (1) establishing whether subduction initiation was spontaneous or induced; (2) if induced, constraining the timing and direction of incipient plate convergence and (3) reconstructing the entire plate boundary from triple junction to triple junction, as well as the boundaries of neighbouring plates, to identify collisions, subduction terminations or mantle plume arrival that may have caused stress changes driving subduction initiation. In this paper, to evaluate the driver of subduction initiation and plate boundary formation, we provide such an analysis for an intra-oceanic subduction zone that formed within the Neotethys Ocean around 105 Myr ago (Ma).

Induced subduction initiation across the Neotethys Ocean

During induced subduction initiation, lower plate burial, dated through prograde mineral growth in rocks of the incipient subduction plate contact, in so-called metamorphic soles⁸ predates upper plate extension that is inferred from spreading records in so-called supra-subduction zone (SSZ) ophiolites^{9–11}. Such SSZ ophiolites have a chemical stratigraphy widely interpreted as having formed at spreading ridges above a nascent subduction zone. Several SSZ ophiolite belts exist in the Alpine–Himalayan mountain belt, which formed during the closure of the Neotethys Ocean^{12,13} (Fig. 1a). One of these ophiolite belts formed during the Cretaceous period and runs from the eastern Mediterranean region along northern Arabia to Pakistan. Incipient lower plate burial has been dated through Lu/Hf prograde garnet growth ages of ~104 Ma in metamorphic soles in Oman as well as in the eastern Mediterranean region^{8,14}. Upper plate extension and SSZ ophiolite spreading have been dated using magmatic zircon U/Pb ages and synchronous metamorphic sole ⁴⁰Ar–³⁹Ar cooling ages and occurred at 96–95 Ma (Pakistan, Oman)^{15,16} to 92–90 Ma (Iran, eastern Mediterranean region)¹⁷. The 8–14 Myr time delay between initial lower plate burial and upper plate extension demonstrates that subduction initiation was induced⁸.

An initial ~E–W convergence direction at this subduction zone was constrained through palaeomagnetic analysis and detailed kinematic reconstruction of post-subduction initiation deformation of the eastern Mediterranean region, Oman and Pakistan and was accommodated at ~N–S striking trench segments^{13,18–20}. This is surprising: for hundreds of millions of years and throughout the Tethyan realm, rifts and ridges accommodated the separation of continental fragments off northern Gondwana in the south and

¹Department of Earth Sciences, Utrecht University, Utrecht, The Netherlands. ²GFZ German Research Centre for Geosciences, Potsdam, Germany. ³Centre of Earth Evolution and Dynamics (CEED), University of Oslo, Oslo, Norway. ⁴Département de Géologie et de Génie Géologique, Université Laval, Québec, Québec, Canada. ⁵School of Geography, Earth and Environmental Sciences, University of Birmingham, Birmingham, UK. ⁶School of Earth and Environmental Sciences, University of Queensland, St Lucia, Queensland, Australia. ⁷BRGM, Orléans, France. ⁸School for Earth and Atmospheric Sciences, Queensland University of Technology, Brisbane, Queensland, Australia. ✉e-mail: d.j.j.vanhinsbergen@uu.nl

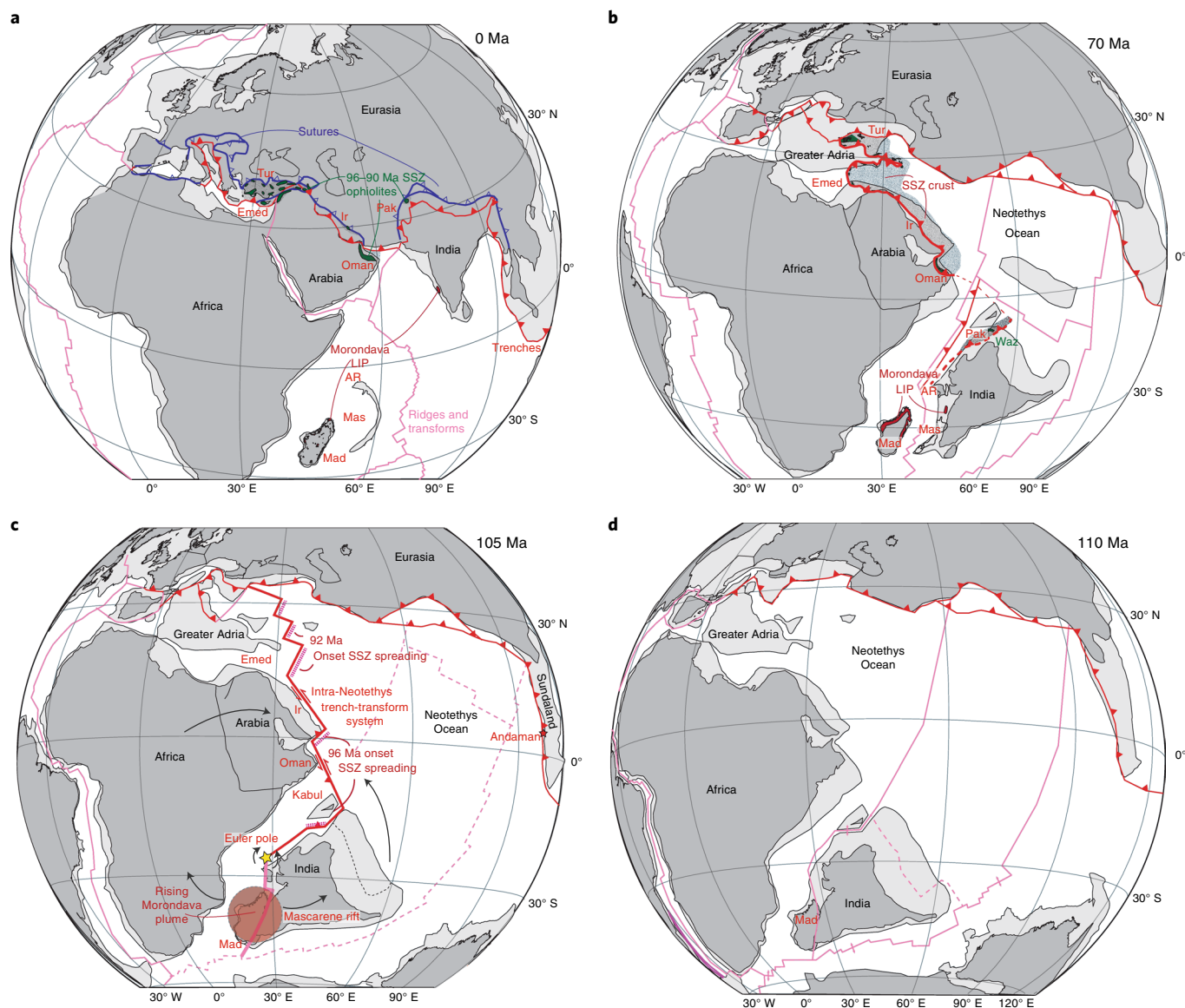


Fig. 1 | Plate kinematic reconstructions of the Neotethys Ocean and surrounding continents. a–d, Reconstructions of the present day (**a**); 70 Ma (**b**); 105 Ma (**c**), corresponding to the timing of intra-Neotethyan subduction initiation; and 110 Ma (**d**), just before intra-Neotethyan subduction initiation. In **c**, the black arrows indicate rotation direction around the Euler pole indicated by the yellow star. See Methods for the plate reconstruction approach and sources of detailed restorations. Reconstructions are shown in a mantle reference frame⁴⁵. AR, Amirante Ridge; Emed, Eastern Mediterranean Region; Ir, Iran; LIP, Large Igneous Province; Mad, Madagascar; Mas, Mascarene Basin; Pak, Pakistan, Tur, Turkey; Waz, Waziristan Ophiolite.

their northward migration, until they accreted at subduction zones along the southern Eurasian margin^{21,22}. The ~E–W convergence that triggered ~105 Ma subduction initiation across the Neotethys Ocean was thus near-orthogonal to the long-standing plate motions. To find the trigger inducing this subduction, we developed the first comprehensive reconstruction of the entire ~12,000-km-long plate boundary that formed at ~105 Ma and placed this in context of reconstructions of collisions and mantle plumes of the Neotethyan realm (Fig. 1).

Geological reconstruction of incipient plate boundary

The SSZ ophiolites that formed at the juvenile Cretaceous intra-Neotethyan subduction zone are now found as klippen on intensely deformed accretionary orogenic belts (Fig. 1a) that formed when the continents of Greater Adria, Arabia and India arrived in subduction zones. We reconstructed these orogenic belts (Fig. 1)

and restored these continents, and the Cretaceous ophiolites that were thrust upon these, into their configuration at 105 Ma (Fig. 1c) (Methods).

The westernmost geological record of the Cretaceous intra-Neotethyan subduction zone is found in eastern Greece and western Turkey, where it ended in a trench–trench–trench triple junction with subduction zones along the southern Eurasian margin¹⁸. From there, east-dipping (in the west) and west-dipping (in the east) subduction segments followed the saw-toothed shape of the Greater Adriatic and Arabian continental margins (Fig. 1c) and initiated close to it: rocks of these continental margins had already underthrust the ophiolites within 5–15 Myr after SSZ ophiolite spreading^{14,23,24}, and continent-derived zircons have been found in metamorphic sole rocks²⁵. Subduction segments likely nucleated along ancient N–S and NE–SW trending fracture zones and linked through highly oblique, north-dipping subduction zones that

trended parallel to and likely reactivated the pre-existing (hyper) extended passive margins (Fig. 1b,c)^{20,23}. Subducted remnants of the Cretaceous intra-Neotethyan subduction are well resolved in the present-day mantle as slabs in the mid-mantle below the southeastern Mediterranean Sea, central Arabia and the west Indian Ocean²⁶.

East of Arabia, we trace the intra-oceanic plate boundary to a NE–SW striking, NW-dipping subduction zone between the Kabul Block and the west Indian passive margin. The 96 Ma Waziristan ophiolites of Pakistan formed above this subduction zone, perhaps by inverting an Early Cretaceous spreading ridge between the Kabul Block and India¹³ and were thrust eastward onto the Indian margin^{13,16} (Fig. 1b,c). The Cretaceous intra-Neotethyan plate boundary may have been convergent to the Amirante Ridge in the west Indian Ocean¹³, from where it became extensional instead and developed a rift, and later a spreading ridge, in the Mascarene Basin that accommodated separation of India from Madagascar^{13,27,28} (Fig. 1b). The plate boundary ended in a ridge–ridge–ridge triple junction in the south Indian Ocean^{13,28} (Fig. 1b).

The newly formed Cretaceous plate boundary essentially temporarily merged a large part of Neotethyan oceanic lithosphere between Arabia and Eurasia to the Indian plate. This plate was >12,000 km long from triple junction to triple junction and reached from 45° S to 45° N, with 4,500 km of rift/ridge in the southeast and 7,500 km of subduction zone in the northwest and with a transition between the convergent and divergent segments, representing the India–Africa Euler pole¹³, in the west Indian Ocean, at a latitude between Pakistan and the Amirante Ridge (Fig. 1b). Marine geophysical constraints show a ~4° counterclockwise rotation of India relative to Africa about the west Indian Ocean Euler pole during rifting preceding the ~83 Ma onset of oceanic spreading in the Mascarene Basin^{27–29}, associated with up to hundreds of kilometres of ~E–W convergence across the Neotethys (Fig. 1d).

The neighbouring plates of the intra-Neotethyan subduction zone at 105 Ma were thus Africa and India. The African plate was mostly surrounded by ridges and had a complex subduction plate boundary in the Mediterranean region³⁰. The Indian plate was surrounded by ridge-transform systems in the south and east and by subduction in the north and may have contained rifts and ridges between the Indian continent and Eurasia^{13,28}. The Neotethys lithosphere between Arabia–Greater Adria and Eurasia continued unbroken to the north-dipping subduction zone that had already existed along the southern Eurasian margin since the Jurassic^{31,32}: the spreading ridges that existed during Neotethys Ocean opening in the Permian–Triassic (north of Arabia)³³ and Triassic–Jurassic (eastern Mediterranean region)²³ had already subducted below Eurasia before 105 Ma (refs. ^{19,33}) (Fig. 1b,c).

Identifying potential drivers of subduction initiation

Candidate processes to trigger the reconstructed plate boundary formation at 105 Ma are terminations of existing subduction zones by arrival of buoyant lithosphere or the rise of mantle plumes. Southern Eurasia contains relics of many microcontinents that accreted at or clogged subduction zones since the Palaeozoic, but none of these events started or ended around 105 Ma (refs. ^{13,21–23,33–35}). Continental subduction and collision were ongoing in the central Mediterranean region²³, but it is not evident how this or any other changes in subduction dynamics along the E–W trending southern Eurasian margin would lead to E–W convergence in the Neotethys Ocean. In the eastern Neotethys, a mid-Cretaceous collision of the intra-oceanic Woyla Arc with the Sundaland continental margin led to a subduction polarity reversal initiating eastward subduction below Sundaland³⁶, which is recorded in ophiolites on the Andaman Islands. There, metamorphic sole rocks with ⁴⁰Ar–³⁹Ar hornblende cooling ages of 105–106 Ma and likely coeval SSZ ophiolite spreading ages³⁷ reveal that this subduction zone may have developed slab pull around the same time as the Indian Ocean/western Neotethys

plate boundary formed (Fig. 1c). However, eastward slab pull below Sundaland cannot drive E–W convergence in the Neotethys to the west, and Andaman SSZ extension may well be an expression rather than the trigger of Indian plate rotation. We find no viable plate tectonics-related driver of the ~105 Ma plate boundary formation that we reconstructed here.

However, a key role is possible for the only remaining geodynamic, non-plate-tectonic plate-motion driver in the region: a mantle plume. India–Madagascar continental break-up is widely viewed^{13,27,37} as related to the ~94 Ma and younger formation of the Morondava large igneous province (LIP) on Madagascar³⁸ and southwest India³⁹. This LIP, however, started forming ~10 Myr after initial plate boundary formation. To understand whether the plume may be responsible for both LIP emplacement and plate boundary formation, we explore existing numerical models of plume–plate interaction and conduct explorative torque balance simulations of plume–lithosphere interaction.

Mantle plumes driving subduction initiation

Numerical simulations of plume–lithosphere interaction have already identified that plume-head spreading below the lithosphere leads to horizontal asthenospheric flow that exerts a ‘plume push’ force on the base of the lithosphere, particularly in the presence of a cratonic keel^{5,40,41}. Plume push may accelerate plates by several cm yr⁻¹ (ref. ⁴¹) and has been proposed as a potential driver of subduction initiation⁵.

In many cases, including in the case of the Morondava LIP, LIP eruption and emplacement shortly preceded continental break-up, but pre-break-up rifting preceded LIP emplacement by 10–15 Myr (ref. ²⁷). This early rifting typically is interpreted to indicate that the plume migrated along the base of the lithosphere into a pre-existing rift that formed independently of plume rise²⁷. However, in numerical simulations dynamic uplift⁴² and plume push⁴¹ have already started to accelerate plates 10–15 Myr before the plume head reaches the base of the lithosphere and emplaces the LIP. Numerical simulations thus predict the observed delay between plume push as a driver for early rifting and subduction initiation and LIP eruption and emplacement.

Here, we add to these plume–lithosphere coupling experiments by conducting proof-of-concept torque balance simulations exploring, in particular, why the observed India–Africa Euler pole is so close to the plume head such that the associated plate rotation between Africa and India caused E–W convergence in the Neotethys. We performed semi-analytical computations, including both the Indian and African plates at ~105 Ma, and assessed the influence of cratonic keels on the position of the India–Africa Euler pole (Fig. 2 and Methods).

In our computations without cratonic keels, plume push under Madagascar/India caused counterclockwise rotation of India versus Africa, but about an Euler pole situated far north of Arabia (Fig. 2a), without inducing notable E–W convergence within the Neotethys. However, in experiments that include keels of the Indian and African cratonic lithosphere, which are strongly coupled to the sub-asthenospheric mantle, the computed Euler pole location is shifted southward towards the Indian continent, inducing E–W convergence along a larger part of the plate boundary within the Neotethys Ocean (Fig. 2b).

Convergence of up to several hundreds of kilometres, sufficient to induce self-sustaining subduction²⁷, is obtained if plume material is fed into—and induced flow is confined to—a 200 km-thick weak asthenospheric layer. The thinner this layer is, the further the plume head spreads and pushes the plate. The modern Indian cratonic root used in our computations has likely eroded considerably during interaction with the ~70–65 Ma Deccan plume⁴³. India may have had a thicker and/or laterally more extensive cratonic root at ~105 Ma than modelled here, which would further enhance

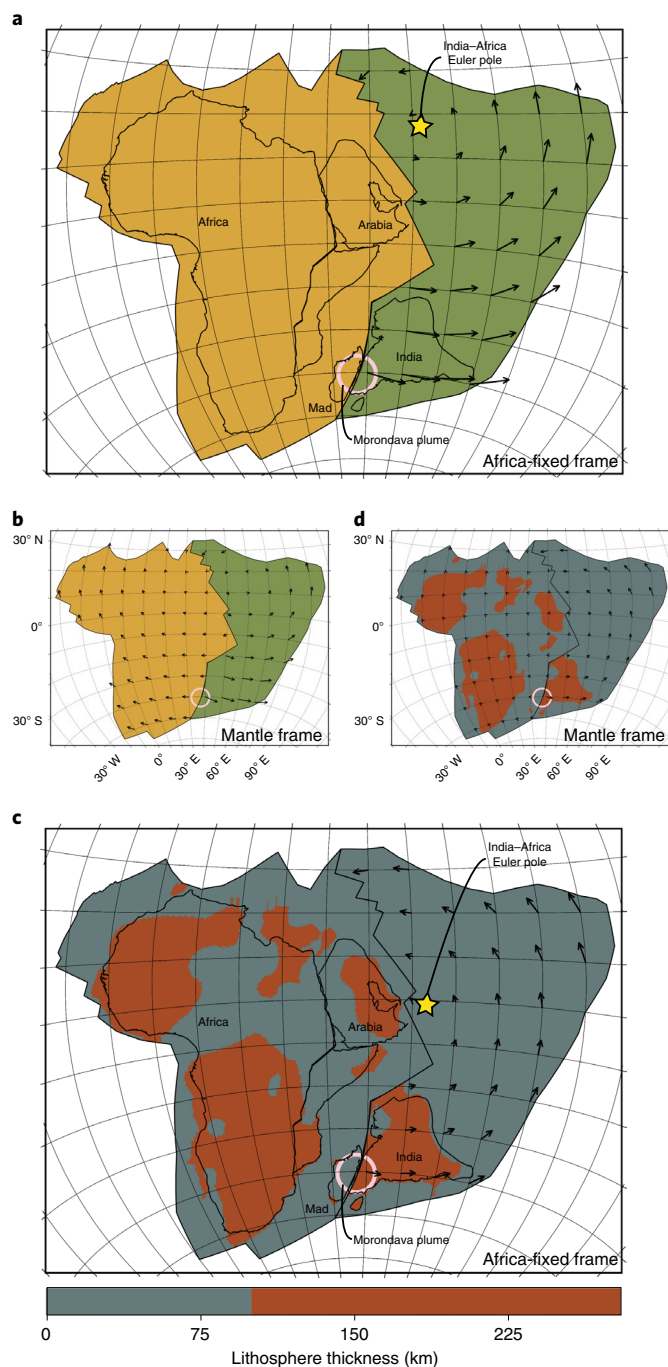


Fig. 2 | Torque balance modelling results of plumes affecting plates similar to India and Africa with and without cratonic keels.

a–d. The computed total displacement (black arrows) induced by the Morondava plume (pink circle) for the restored ~105 Ma plate configuration (Fig. 1c) for plates without (**a,b**) and with (**c,d**) African and Indian cratonic keels, in an Africa-fixed (**a,c**) or mantle (**b,d**) reference frame⁴⁵ (Methods). Ten-degree grid spacing; locations of plates, lithosphere thickness and the plume are reconstructed in a slab-fitted mantle reference frame⁴⁵.

coupling of the lithosphere and the sub-asthenospheric mantle. Furthermore, an Euler pole close to India and a long convergent boundary to the north requires much weaker coupling in the northern (oceanic) part of the India plate (Fig. 2). In this case, results remain similar as long as the plume impinges near the southern part of the western boundary of continental India.

An order-of-magnitude estimate of the maximum plume-induced stresses, assuming no frictional resistance at other plate boundaries, is obtained from the rising force of $\sim 1.5 \times 10^{20}$ N of a plume head with a 1,000 km diameter and 30 kg m^{-3} density contrast. If half of this force acts on the India plate and with a lever arm of 4,000 km, this corresponds to a torque of 3×10^{26} N m. Once ridge push is established, at the onset of rifting, as an additional force in the vicinity of the plume, we estimate that this number may increase by up to a few tens of per cent. This torque can be balanced at the convergent boundary (length $\sim 5,000$ km, plate thickness ~ 100 km) involving stresses of ~ 240 MPa, much larger than estimates of frictional resistance between subducting and overriding plates that are only of the order of tens of MPa (ref. 44). For this estimate, we neglect any frictional resistance at the base of the plate and at any other plate boundary, essentially considering the plate as freely rotating above a pinning point. This is another end-member scenario, as opposed to our above convergence estimate where we had considered friction at the plate base but neglected it at all plate boundaries. Therefore, the estimate of 240 MPa may be considered as an upper bound, but being compressive and oriented in the right direction, it shows the possibility of subduction initiation as has occurred in reality along the likely weakened passive margin region of Arabia and Greater Adria. Moreover, the plume-induced compressive stresses may have added to pre-existing compressive stresses, in particular due to ridge push around the African and Indian plates. Such additional compressive stresses may contribute to shifting the Euler pole further south, closer to the position reconstructed in Fig. 1.

Subduction became self-sustained ~ 8 – 12 Myr after its initiation, as marked by the 96–92 Ma age of SSZ spreading^{15,17}; inception of this spreading shows that subduction rates exceeded convergence rates, and reconstructed SSZ spreading rates were an order of magnitude higher¹⁵ than Africa–Arabia or Indian absolute plate motions^{41,45}, signalling slab rollback (that is, self-sustained subduction^{20,46}). Numerical models suggest that self-sustained subduction may start after ~ 50 – 100 km of induced convergence⁷, corresponding to $\sim 1^\circ$ of India–Africa rotation between ~ 105 and ~ 96 – 92 Ma. Subsequent east- and west-dipping subduction segments (Fig. 1) may have contributed to and accelerated the India–Africa/Arabia rotation, driving the propagation of the Euler pole farther to the south (compare Fig. 2a,c).

Mantle plumes as an initiator of plate tectonics?

Previously, numerical modelling has shown that mantle plumes may trigger circular subduction initiation around a plume head⁴, where local plume-related convection may drive subduction of thermally weakened lithosphere. This subduction would propagate through slab rollback and may have started the first subduction features on Earth⁴. Three-dimensional convective models do produce a global network of plate boundaries^{47,48}, but the role of plumes in initiating new subduction zones within this network is unclear. Here we have provided the first evidence that plume rise formed a $>12,000$ -km-long plate boundary composed of both convergent and divergent segments. Our documented example is Cretaceous in age, but geological observations showing a general temporal overlap between LIP emplacement and formation of SSZ ophiolite belts over more than a billion years⁴⁹ suggest that plume rise is a key driving factor in the formation of subduction plate boundaries. Because mantle plumes are thought to also be common features on planets without plate tectonics, such as Mars and Venus⁵⁰, they may have played a vital role in the emergence of modern-style plate tectonics on Earth. That plumes may have been key for the evolution of plate tectonics on Earth, as we suggest, but apparently insufficient on Mars and Venus, provides a new outlook on understanding the different planetary evolutions.

Online content

Any methods, additional references, Nature Research reporting summaries, source data, extended data, supplementary information, acknowledgements, peer review information; details of author contributions and competing interests; and statements of data and code availability are available at <https://doi.org/10.1038/s41561-021-00780-7>.

Received: 10 July 2020; Accepted: 26 May 2021;

Published online: 8 July 2021

References

- Lenardic, A. The diversity of tectonic modes and thoughts about transitions between them. *Phil. Trans. A* **376**, 20170416 (2018).
- Stern, R. J. Subduction initiation: spontaneous and induced. *Earth Planet. Sci. Lett.* **226**, 275–292 (2004).
- Hall, C. E., Gurnis, M., Sdrolias, M., Lavier, L. L. & Müller, R. D. Catastrophic initiation of subduction following forced convergence across fracture zones. *Earth Planet. Sci. Lett.* **212**, 15–30 (2003).
- Gerya, T. V., Stern, R. J., Baes, M., Sobolev, S. V. & Whattam, S. A. Plate tectonics on the Earth triggered by plume-induced subduction initiation. *Nature* **527**, 221–225 (2015).
- Pusok, A. E. & Stegman, D. R. The convergence history of India–Eurasia records multiple subduction dynamics processes. *Sci. Adv.* **6**, eaaz8681 (2020).
- Baes, M., Sobolev, S., Gerya, T. & Brune, S. Plume-induced subduction initiation: single-slab or multi-slab subduction? *Geochem. Geophys. Geosyst.* **21**, e2019GC008663 (2020).
- Gurnis, M., Hall, C. & Lavier, L. Evolving force balance during incipient subduction. *Geochem. Geophys. Geosyst.* **5**, Q07001 (2004).
- Guilmette, C. et al. Forced subduction initiation recorded in the sole and crust of the Semail Ophiolite of Oman. *Nat. Geosci.* **11**, 688–695 (2018).
- Stern, R. J. & Gerya, T. Subduction initiation in nature and models: a review. *Tectonophysics* <https://doi.org/10.1016/j.tecto.2017.10.014> (2017).
- Agard, P. et al. Plate interface rheological switches during subduction infancy: control on slab penetration and metamorphic sole formation. *Earth Planet. Sci. Lett.* **451**, 208–220 (2016).
- van Hinsbergen, D. J. J. et al. Dynamics of intraoceanic subduction initiation: 2. Suprasubduction zone ophiolite formation and metamorphic sole exhumation in context of absolute plate motions. *Geochem. Geophys. Geosyst.* **16**, 1771–1785 (2015).
- Dilek, Y. & Furnes, H. Ophiolite genesis and global tectonics: geochemical and tectonic fingerprinting of ancient oceanic lithosphere. *Geol. Soc. Am. Bull.* **123**, 387–411 (2011).
- Gaina, C., van Hinsbergen, D. J. J. & Spakman, W. Tectonic interactions between India and Arabia since the Jurassic reconstructed from marine geophysics, ophiolite geology, and seismic tomography. *Tectonics* **34**, 875–906 (2015).
- Pourteau, A. et al. Thermal evolution of an ancient subduction interface revealed by Lu–Hf garnet geochronology, Halilbaği Complex (Anatolia). *Geosci. Front.* **10**, 127–148 (2019).
- Rioux, M. et al. Synchronous formation of the metamorphic sole and igneous crust of the Semail ophiolite: new constraints on the tectonic evolution during ophiolite formation from high-precision U–Pb zircon geochronology. *Earth Planet. Sci. Lett.* **451**, 185–195 (2016).
- Robinson, J., Beck, R., Gnos, E. & Vincent, R. K. New structural and stratigraphic insights for northwestern Pakistan from field and Landsat Thematic Mapper data. *Geol. Soc. Am. Bull.* **112**, 364–374 (2000).
- Parlak, O. The tauride ophiolites of Anatolia (Turkey): a review. *J. Earth Sci.* **27**, 901–934 (2016).
- van Hinsbergen, D. J. J. et al. Tectonic evolution and paleogeography of the Kırşehir Block and the Central Anatolian Ophiolites, Turkey. *Tectonics* **35**, 983–1014 (2016).
- Maffione, M., van Hinsbergen, D. J. J., de Gelder, G. I. N. O., van der Goes, F. C. & Morris, A. Kinematics of Late Cretaceous subduction initiation in the Neo-Tethys Ocean reconstructed from ophiolites of Turkey, Cyprus, and Syria. *J. Geophys. Res. Solid Earth* **122**, 3953–3976 (2017).
- van Hinsbergen, D. J., Maffione, M., Koornneef, L. M. & Guilmette, C. Kinematic and paleomagnetic restoration of the Semail ophiolite (Oman) reveals subduction initiation along an ancient Neotethyan fracture zone. *Earth Planet. Sci. Lett.* **518**, 183–196 (2019).
- Torsvik, T. H. & Cocks, L. R. M. *Earth History and Palaeogeography* (Cambridge Univ. Press, 2017).
- Wan, B. et al. Cyclical one-way continental rupture-drift in the Tethyan evolution: subduction-driven plate tectonics. *Sci. China Earth Sci.* **62**, 2005–2016 (2019).
- van Hinsbergen, D. J. J. et al. Orogenic architecture of the Mediterranean region and kinematic reconstruction of its tectonic evolution since the Triassic. *Gondwana Res.* **81**, 79–229 (2020).
- Warren, C. J., Parrish, R. R., Waters, D. J. & Searle, M. P. Dating the geologic history of Oman's Semail ophiolite: insights from U–Pb geochronology. *Contrib. Mineral. Petrol.* **150**, 403–422 (2005).
- Güngör, T. et al. Kinematics and U–Pb zircon ages of the sole metamorphics of the Marmaris Ophiolite, Lycian Nappes, Southwest Turkey. *Int. Geol. Rev.* **61**, 1124–1142 (2019).
- van der Meer, D. G., van Hinsbergen, D. J. J. & Spakman, W. Atlas of the underworld: slab remnants in the mantle, their sinking history, and a new outlook on lower mantle viscosity. *Tectonophysics* **723**, 309–448 (2018).
- Buiter, S. J. & Torsvik, T. H. A review of Wilson Cycle plate margins: a role for mantle plumes in continental break-up along sutures? *Gondwana Res.* **26**, 627–653 (2014).
- Gibbons, A. D., Whittaker, J. M. & Müller, R. D. The breakup of East Gondwana: assimilating constraints from Cretaceous ocean basins around India into a best-fit tectonic model. *J. Geophys. Res. Solid Earth* **118**, 808–822 (2013).
- Gaina, C., Müller, R. D., Brown, B., Ishihara, T. & Ivanov, S. Breakup and early seafloor spreading between India and Antarctica. *Geophys. J. Int.* **170**, 151–169 (2007).
- Gaina, C. et al. The African Plate: a history of oceanic crust accretion and subduction since the Jurassic. *Tectonophysics* **604**, 4–25 (2013).
- Agard, P., Jolivet, L., Vrielynck, B., Burrov, E. & Monié, P. Plate acceleration: the obduction trigger? *Earth Planet. Sci. Lett.* **258**, 428–441 (2007).
- Jolivet, L. et al. Neo-Tethys geodynamics and mantle convection: from extension to compression in Africa and a conceptual model for obduction. *Can. J. Earth Sci.* **53**, 1190–1204 (2015).
- Stampfli, G. M. & Borel, G. A plate tectonic model for the Paleozoic and Mesozoic constrained by dynamic plate boundaries and restored synthetic oceanic isochrons. *Earth Planet. Sci. Lett.* **196**, 17–33 (2002).
- van Hinsbergen, D. J. J. et al. Reconstructing Greater India: paleogeographic, kinematic, and geodynamic perspectives. *Tectonophysics* **760**, 69–94 (2019).
- Kapp, P. & DeCelles, P. G. Mesozoic–Cenozoic geological evolution of the Himalayan–Tibetan orogen and working tectonic hypotheses. *Am. J. Sci.* **319**, 159–254 (2019).
- Advokaat, E. L. et al. Early Cretaceous origin of the Woyle Arc (Sumatra, Indonesia) on the Australian plate. *Earth Planet. Sci. Lett.* **498**, 348–361 (2018).
- Plunder, A. et al. History of subduction polarity reversal during arc-continent collision: constraints from the Andaman Ophiolite and its metamorphic sole. *Tectonics* **39**, e2019TC005762 (2020).
- Torsvik, T. et al. Late Cretaceous magmatism in Madagascar: palaeomagnetic evidence for a stationary Marion hotspot. *Earth Planet. Sci. Lett.* **164**, 221–232 (1998).
- Mohan, M. R. et al. The Ezhimala igneous complex, southern India: possible imprint of late Cretaceous magmatism within rift setting associated with India–Madagascar separation. *J. Asian Earth Sci.* **121**, 56–71 (2016).
- Cande, S. C. & Stegman, D. R. Indian and African plate motions driven by the push force of the Reunion plume head. *Nature* **475**, 47–52 (2011).
- van Hinsbergen, D. J. J., Steinberger, B., Doubrovine, P. V. & Gassmöller, R. Acceleration and deceleration of India–Asia convergence since the Cretaceous: roles of mantle plumes and continental collision. *J. Geophys. Res.* <https://doi.org/10.1029/2010jb008051> (2011).
- Wang, Y. & Li, M. The interaction between mantle plumes and lithosphere and its surface expressions: 3-D numerical modelling. *Geophys. J. Int.* <https://doi.org/10.1093/gji/ggab014> (2021).
- Kumar, P. et al. The rapid drift of the Indian tectonic plate. *Nature* **449**, 894–897 (2007).
- Lamb, S. & Davis, P. Cenozoic climate change as a possible cause for the rise of the Andes. *Nature* **425**, 792–797 (2003).
- van der Meer, D. G., Spakman, W., van Hinsbergen, D. J. J., Amaru, M. L. & Torsvik, T. H. Towards absolute plate motions constrained by lower-mantle slab remnants. *Nat. Geosci.* **3**, 36–40 (2010).
- Tavani, S., Corradetti, A., Sabbatino, M., Seers, T. & Mazzoli, S. Geological record of the transition from induced to self-sustained subduction in the Oman Mountains. *J. Geodyn.* **133**, 101674 (2020).
- Tackley, P. J. Mantle convection and plate tectonics: toward an integrated physical and chemical theory. *Science* **288**, 2002–2007 (2000).
- Coltice, N., Husson, L., Faccenna, C. & Arnould, M. What drives tectonic plates? *Sci. Adv.* **5**, eaax4295 (2019).
- Dilek, Y. Ophiolite pulses, mantle plumes and orogeny. *Geol. Soc. Lond. Spec. Publ.* **218**, 9–19 (2003).
- Ernst, R., Grosfils, E. & Mege, D. Giant dike swarms: Earth, Venus, and Mars. *Annu. Rev. Earth Planet. Sci.* **29**, 489–534 (2001).

Publisher's note Springer Nature remains neutral with regard to jurisdictional claims in published maps and institutional affiliations.

© The Author(s), under exclusive licence to Springer Nature Limited 2021

Methods

Kinematic reconstruction. The kinematic restoration of Neotethyan intra-oceanic subduction was made in GPlates plate reconstruction software (www.gplates.org)⁵¹. First, we systematically restored stable plates using marine geophysical data from the Atlantic and Indian Ocean, and then we restored continental margin deformation that occurred following the arrival of continental lithosphere below the oceanic lithosphere preserved as ophiolites. These restorations are based on a systematic reconstruction protocol, based on magnetic anomalies and fracture zones of present-day sea floor and geophysical constraints on pre-drift extension in adjacent passive continental margins²³, followed by kinematic restoration of post-obduction orogenic deformation using structural geological constraints on continental extension, strike-slip deformation and shortening as well as palaeomagnetic constraints on vertical axis rotations. We then restored pre-emplacement vertical axis microplate rotations^{52,53} as well as palaeo-orientations of the SSZ spreading ridges at which the ophiolitic crust formed^{18–20}. The reconstruction shown in Fig. 1b compiles kinematic restorations for the eastern Mediterranean region²³, Iran⁵⁴, Oman²⁰, Pakistan¹³ and the Himalaya⁵⁴. Ophiolites interpreted to be part of the Cretaceous subduction system include the 96–90 Ma Cretaceous ophiolites exposed in SE Greece, Anatolia, Cyprus, Syria and Iraq; the Neyriz ophiolite of Iran; the Semail ophiolite in Oman and the Waziristan–Khost ophiolite in Pakistan and Afghanistan^{15–17,55}. The Jurassic ophiolite belts of northern Turkey and Armenia^{56–58} and the Late Cretaceous (<80 Ma) Kermanshah ophiolite of Iran⁵⁹ are not included and are instead interpreted to have formed along the southern Eurasian margin²³. The Masirah Ophiolite of East Oman⁶⁰ and the uppermost Cretaceous Bela, Muslim Bagh and Kabul–Altimur ophiolites of Pakistan and Afghanistan^{61,62} are interpreted to reflect oblique latest Cretaceous to Palaeogene India–Arabia convergence¹³ and are also unrelated to the event studied here. Restoration of intra-oceanic subduction prior to the arrival of the continental margins used palaeomagnetic data from the ophiolites of Oman, Syria, Cyprus and Turkey that constrain vertical axis rotations, as well as the orientation of sheeted dyke following cooling after intrusion^{18–20,52,53} as a proxy for original ridge and intra-oceanic trench orientations. These palaeomagnetic data systematically revealed N–S to NW–SE primary sheeted dyke orientations^{18–20,52,53}. Because the ages of the SSZ ophiolites in the Neotethyan belt do not laterally progress, spreading must have occurred near-orthogonal to the associated trench, which must thus also have been striking N–S to NE–SW, as shown in the reconstruction of Fig. 1.

How far the Indian plate continued northwards around 105 Ma is subject to ongoing debate. The northern Indian continental margin has been proposed to have rifted off India sometime in the Cretaceous^{34,63}, but recent palaeomagnetic data suggest that this process occurred in the Late Cretaceous, well after 100 Ma (ref. 64). Others inferred that the north Indian continent had a passive margin contiguous with oceanic Neotethyan lithosphere since the middle Jurassic or before and continued to a subduction zone below the SSZ ophiolites found in the Himalayan suture zone and the Kohistan arc^{35,65,66}. Sedimentary and palaeomagnetic data demonstrate that these ophiolites formed adjacent to the Eurasian margin in the Early Cretaceous⁶⁷, although they may have migrated southward during slab rollback in the Late Cretaceous³⁵. Recent palaeomagnetic data have shown that a subduction zone may have existed within the Neotethys to the west of the Andaman Islands, above which the West Burma Block would have been located (Fig. 1)⁶⁸. Our reconstruction of the eastern Neotethys may thus be oversimplified. However, the geological record of the West Burma Block shows that this subduction zone already existed as early as 130 Ma and was E–W trending until well into the Cenozoic⁶⁸, and we see no reason to infer that changes in the eastern Neotethys contributed to the plate boundary formation discussed here. Some have speculated that the West Burma subduction zone would have been connected to a long-lived, equatorial subduction zone within the Neotethys all along the Indian segment that would already have existed in the Early Cretaceous⁶⁹: this scenario remains unconstrained by palaeomagnetic data and is inconsistent with sediment provenance data from the Himalaya and overlying ophiolites³⁵. In summary, around 105 Ma, the Indian plate continued far into the Neotethyan realm, and the India–Africa rotation is a likely driver of E–W convergence sparking subduction initiation close to the northern Gondwana margin purported in Fig. 1.

Torque balance modelling. Forces considered here include (1) the push due to plume-induced flow in the asthenosphere and (2) the drag due to shear flow between the moving plate and a deeper mantle at rest (Supplementary Fig. 1). In the first case, we disregard any lateral variations. Plume-induced flow is treated as Poiseuille flow (that is, with parabolic flow profile) in an asthenospheric channel of thickness h , radially away from the plume stem. Since at greater distance plume-induced flow will eventually not remain confined to the asthenosphere, we only consider it to a distance of 2,400 km, in accordance with numerical results⁴¹ and consistent with the finding that there is a transition from dominantly pressure-driven Poiseuille flow at shorter wavelengths to dominantly shear-driven Couette flow at length scales approximately exceeding mantle depth^{70,71}. With v_0 the velocity in the centre of the channel at a distance d from the plume stem, the total volume flux rate is $2/3 \times v_0 \times 2\pi d \times h_c$ (here neglecting the curvature of the Earth surface for simplicity). Its time integral is equal to the volume of the plume head

with radius estimated⁷² to be about $r_p = 500$ km, with considerable uncertainty. That is, integration is done over a time interval until the entire plume-head volume has flowed into the asthenospheric channel. Hence the corresponding displacement vector in the centre of the channel is

$$\mathbf{x}_{\text{plu}} = \int_{\Delta t} v_0 dt \mathbf{e}_r = \frac{r_p^3}{dh_c} \mathbf{e}_r$$

where \mathbf{e}_r is the unit vector radially away from the plume (red arrows in Supplementary Fig. 1). Because of the parabolic flow profile, the vertical displacement gradient at the top of the channel is

$$2 \frac{\mathbf{x}_{\text{plu}}}{0.5h_c} = \frac{4}{h_c} \int_{\Delta t} v_0 dt \mathbf{e}_r = \frac{4r_p^3}{dh_c^2} \mathbf{e}_r.$$

Viscosity is defined such that the force per area is equal to viscosity times the radial gradient of horizontal velocity. Hence the time integral of torque on the plate is

$$\mathbf{T}_{\text{plu}} = \frac{4\eta_0}{h_c} \int_A \mathbf{r} \times \mathbf{x}_{\text{plu}} dA = \frac{4\eta_0 r_p^3}{dh_c^2} \int_A \mathbf{r} \times \mathbf{e}_r dA$$

where η_0 is viscosity in the channel and \mathbf{r} is the position vector. \mathbf{T}_{plu} is balanced by the time-integrated torque \mathbf{T}_{pla} of the plate rotating an angle $\boldsymbol{\omega}$ over the underlying mantle. With plate displacement vectors $\mathbf{x}_{\text{pla}} = \boldsymbol{\omega} \times \mathbf{r}$ (black arrows in Supplementary Fig. 1) we obtain

$$\mathbf{T}_{\text{pla}} = -\frac{\eta_0}{h_s} \int_A \mathbf{r} \times \mathbf{x}_{\text{pla}} dA = -\frac{\eta_0}{h_s} \int_A \mathbf{r} \times (\boldsymbol{\omega} \times \mathbf{r}) dA.$$

Here h_s is an effective thickness of the layer over which shearing occurs, which is calculated below for a stratified viscosity structure (that is, laterally homogeneous coupling of plate and mantle) and which we will set equal to h_c for simplicity. Specifically, with \mathbf{T}_x being the time-integrated torque acting on a plate rotating an angle ω_0 around the x axis

$$\mathbf{T}_x = -\frac{\omega_0 \eta_0}{h_s} \int_A \mathbf{r} \times (\mathbf{e}_x \times \mathbf{r}) dA$$

and \mathbf{T}_y and \mathbf{T}_z defined in analogy, the torque balance equation can be written

$$\mathbf{T}_{\text{plu}} = \frac{\omega_x}{\omega_0} \mathbf{T}_x + \frac{\omega_y}{\omega_0} \mathbf{T}_y + \frac{\omega_z}{\omega_0} \mathbf{T}_z.$$

ω_0 cancels out when \mathbf{T}_x , \mathbf{T}_y and \mathbf{T}_z are inserted. Integrals used to compute these torques only depend on plate geometry, η_0 cancels out in the torque balance and we can solve for the rotation angle vector $\boldsymbol{\omega}$ simply by a 3×3 matrix inversion. In the more general case, where we do not set h_s and h_c equal, $\boldsymbol{\omega}$ is scaled by a factor h_s/h_c .

If a plate moves over a mantle where viscosity varies with depth, then the force per area F/A should be the same at all depths and the radial gradient of horizontal velocity $dv/dz = F/A/\eta(z)$. If we assume that the deep mantle is at rest (that is, it moves slowly compared to plate motions), we further find that plate motion is

$$v_0 = \int_{z_0}^{z(\eta_{\text{max}})} \frac{dv}{dz} dz = \frac{F}{A} \int_{z_0}^{z(\eta_{\text{max}})} \frac{1}{\eta(z)} dz =: \frac{F}{A} \frac{h_s}{\eta_0}. \quad (1)$$

The integration is done from the base of the lithosphere z_0 to the depth where the approximation of the mantle at rest is probably the most closely matched; that is, we choose the viscosity maximum. The last equality is according to the definition of the effective layer thickness, whereby η_0 is the viscosity just below the lithosphere. Solving this equation for h_s for the viscosity structure in Supplementary Fig. 2 and a 100 km-thick lithosphere gives $h_s = 203.37$ km.

The plume location at 27.1° E, 40.4° S is obtained by rotating the centre of the corresponding LIP at 46° E, 26° S and an age 87 Ma (adopted from Doubrovine et al.⁷³) in the slab-fitted mantle reference frame⁴⁵, in which the plate geometries at 105 Ma are also reconstructed.

Results for this case (Fig. 2a) show that a plume pushing one part of a plate may induce a rotation of that plate, such that other parts of that plate may move in the opposite direction. A simple analogy is a sheet of paper pushed, near its bottom left corner, to the right; then, near the top left corner, the sheet will move to the left. With two sheets (plates) on either side, local divergence near the bottom (near the plume) may turn into convergence near the top (at the part of the plate boundary furthest away from the plume). The length of that part of the plate boundary where convergence is induced may increase if one plate is nearly ‘pinned’ at a hinge point slightly NE of the plume, perhaps due to much stronger coupling between plate and mantle. At the times considered here ~105 Ma, the Indian continent, where coupling was presumably stronger, was in the southern part of the Indian

plate, whereas in its north there was a large oceanic part with presumably weaker coupling. Hence the geometry was indeed such that convergence could be induced along a longer part of the plate boundary.

In the second case, we therefore consider lateral variations in the coupling between plate and mantle, corresponding to variations in lithosphere thickness and/or asthenosphere viscosity, by multiplying the drag force (from the first case) at each location with a resistance factor. This factor is a function of lithosphere thickness reconstructed at 105 Ma. On continents, thickness derived from tomography⁷⁴ with slabs removed⁷⁵ is simply backward-rotated. In the oceans, we use thickness (km) = $10 \times (\text{age (Ma)} - 105)^{0.5}$ with ages from present-day Earthbyte age grid version 3.6 (that is, accounting for the younger age and reduced thickness at 105 Ma), besides backward-rotating. To determine the appropriate rotation, the lithosphere (in present-day location) is divided up into India, Africa, Arabia, Somalia and Madagascar (palaeo-)plates, and respective 105 Ma finite rotations from van der Meer et al.⁴⁵ are applied. For the parts of the reconstructed plates where thickness could not be reconstructed in this way—often because this part of the plate has been subducted—we first extrapolate thickness up to a distance $\sim 2.3^\circ$ and then set the thickness to a default value of 80 km for the remaining part. Reconstructed thickness is shown in Supplementary Fig. 4. For the resistance factor as a function of lithosphere thickness, we use two models. Firstly, we use a continuous curve (Supplementary Fig. 3) according to equation (1)

$$\frac{F}{A} = \frac{v_0}{\int_{z_0}^{z(\eta_{\max})} \frac{1}{\eta(z)} dz} \quad (2)$$

with the mantle viscosity model in Supplementary Fig. 2 combined with variable lithosphere thickness z_0 . However, this causes only a minor change in the plate rotations (Supplementary Fig. 4 compared to Fig. 2b). Hence, we also use a stronger variation, further explained in the caption of Fig. 2 and with results shown in Fig. 2c,d.

Data availability

GPlates files with reconstructions used to draft Fig. 1 are provided at https://figshare.com/articles/dataset/van_Hinsbergen_NatureGeo_2021_GPlates_zip/13516727.

Code availability

All codes used in the geodynamic modelling in this study are available at https://figshare.com/articles/software/van_Hinsbergen_et_al_NatureGeo_2021_geodynamics_package/13635089.

References

- Müller, R. D. et al. GPlates: building a virtual Earth through deep time. *Geochem. Geophys. Geosyst.* **19**, 2243–2261 (2018).
- Clube, T. M. L., Creer, K. M. & Robertson, A. H. F. Palaeorotation of the Troodos microplate, Cyprus. *Nature* **317**, 522 (1985).
- Morris, A., Meyer, M., Anderson, M. W. & MacLeod, C. J. Clockwise rotation of the entire Oman ophiolite occurred in a suprasubduction zone setting. *Geology* **44**, 1055–1058 (2016).
- McQuarrie, N. & van Hinsbergen, D. J. J. Retrodeforming the Arabia–Eurasia collision zone: age of collision versus magnitude of continental subduction. *Geology* **41**, 315–318 (2013).
- Monsef, I. et al. Evidence for an early-MORB to fore-arc evolution within the Zagros suture zone: constraints from zircon U–Pb geochronology and geochemistry of the Neyriz ophiolite (South Iran). *Gondwana Res.* **62**, 287–305 (2018).
- Galoyan, G. et al. Geology, geochemistry and ⁴⁰Ar/³⁹Ar dating of Sevan ophiolites (Lesser Caucasus, Armenia): evidence for Jurassic back-arc opening and hot spot event between the South Armenian Block and Eurasia. *J. Asian Earth Sci.* **34**, 135–153 (2009).
- Çelik, Ö. F. et al. Jurassic metabasic rocks in the Kızıllırmak accretionary complex (Kargı region, Central Pontides, Northern Turkey). *Tectonophysics* **672–673**, 34–49 (2016).
- Topuz, G. et al. Jurassic ophiolite formation and emplacement as backstop to a subduction–accretion complex in northeast Turkey, the Refahiye ophiolite, and relation to the Balkan ophiolites. *Am. J. Sci.* **313**, 1054–1087 (2014).
- Ao, S. et al. U–Pb zircon ages, field geology and geochemistry of the Kermanshah ophiolite (Iran): from continental rifting at 79 Ma to oceanic core complex at ca. 36 Ma in the southern Neo-Tethys. *Gondwana Res.* **31**, 305–318 (2016).
- Peters, T. & Mercolli, I. Extremely thin oceanic crust in the Proto-Indian Ocean: evidence from the Masirah ophiolite, Sultanate of Oman. *J. Geophys. Res. Solid Earth* **103**, 677–689 (1998).
- Gnos, E. et al. Bela oceanic lithosphere assemblage and its relation to the Reunion hotspot. *Terra Nova* **10**, 90–95 (1998).
- Tapponnier, P., Mattauer, M., Proust, F. & Cassaigneau, C. Mesozoic ophiolites, sutures, and large-scale tectonic movements in Afghanistan. *Earth Planet. Sci. Lett.* **52**, 355–371 (1981).
- van Hinsbergen, D. J. J. et al. Greater India Basin hypothesis and a two-stage Cenozoic collision between India and Asia. *Proc. Natl Acad. Sci. USA* **109**, 7659–7664 (2012).
- Yuan, J. et al. Rapid drift of the Tethyan Himalaya terrane before two-stage India–Asia collision. *Natl Sci. Rev.* <https://doi.org/10.1093/nsr/nwaa173> (2020).
- Hébert, R. et al. The Indus–Yarlung Zangbo ophiolites from Nanga Parbat to Namche Barwa syntaxes, southern Tibet: first synthesis of petrology, geochemistry, and geochronology with incidences on geodynamic reconstructions of Neo-Tethys. *Gondwana Res.* **22**, 377–397 (2012).
- Zahirovic, S. et al. Tectonic evolution and deep mantle structure of the eastern Tethys since the latest Jurassic. *Earth Sci. Rev.* **162**, 293–337 (2016).
- Huang, W. et al. Lower Cretaceous Xigaze ophiolites formed in the Gangdese forearc: evidence from paleomagnetism, sediment provenance, and stratigraphy. *Earth Planet. Sci. Lett.* **415**, 142–153 (2015).
- Westerweel, J. et al. Burma Terrane part of the Trans-Tethyan arc during collision with India according to palaeomagnetic data. *Nat. Geosci.* **12**, 863–868 (2019).
- Jagoutz, O., Royden, L., Holt, A. F. & Becker, T. W. Anomalously fast convergence of India and Eurasia caused by double subduction. *Nat. Geosci.* **8**, 475–478 (2015).
- Höink, T. & Lenardic, A. Long wavelength convection, Poiseuille–Couette flow in the low-viscosity asthenosphere and the strength of plate margins. *Geophys. J. Int.* **180**, 23–33 (2010).
- Höink, T., Jellinek, A. M. & Lenardic, A. Viscous coupling at the lithosphere–asthenosphere boundary. *Geochem. Geophys. Geosyst.* **12**, Q0AK02 (2011).
- Campbell, I. H. Testing the plume theory. *Chem. Geol.* **241**, 153–176 (2007).
- Doubrovine, P. V., Steinberger, B. & Torsvik, T. H. A failure to reject: testing the correlation between large igneous provinces and deep mantle structures with EDF statistics. *Geochem. Geophys. Geosyst.* **17**, 1130–1163 (2016).
- Steinberger, B. Topography caused by mantle density variations: observation-based estimates and models derived from topography and lithosphere thickness. *Geophys. J. Int.* **205**, 604–621 (2016).
- Steinberger, B. & Becker, T. W. A comparison of lithospheric thickness models. *Tectonophysics* **746**, 325–338 (2018).

Acknowledgements

D.J.J.v.H. acknowledges funding through European Research Council Starting Grant 306810 (SINK) (also funding M.M., D.G., A.P. and E.L.A.), Netherlands Organization for Scientific Research (NWO) Vidi grant 864.11.004 (also funding K.P. and P.J.M.) and Netherlands Organization for Scientific Research (NWO) Vici grant 865.17.001. B.S. and C. Gaina received funding from the Research Council of Norway through its Centres of Excellence funding scheme, project no. 223272. B.S. acknowledges the innovation pool of the Helmholtz Association through the Advanced Earth System Modelling Capacity (ESM) activity. C. Guilmette was funded through Discovery Grant (RGPIN-2014-05681) from the National Science and Engineering Research Council of Canada. We thank I. L. ten Kate and D. Bandyopadhyay for discussion and F. Capitanio and D. Müller for their comments.

Author contributions

D.J.J.v.H., B.S. and W.S. designed the research. D.J.J.v.H., C. Guilmette, M.M., D.G., K.P., A.P., P.J.M., C. Gaina, E.L.A. and R.L.M.V. developed the kinematic reconstruction; B.S. performed modelling; D.J.J.v.H., B.S., C. Guilmette and W.S. wrote the paper and all authors made corrections and edits.

Competing interests

The authors declare no competing interests.

Additional information

Supplementary information The online version contains supplementary material available at <https://doi.org/10.1038/s41561-021-00780-7>.

Correspondence and requests for materials should be addressed to D.J.J.v.H.

Peer review information *Nature Geoscience* thanks R. Dietmar Müller, Fabio Capitanio and the other, anonymous, reviewer(s) for their contribution to the peer review of this work. Primary Handling Editor: Stefan Lachowycz.

Reprints and permissions information is available at www.nature.com/reprints.